Applied Catalysis B: Environmental 128 (2012) 72–76

Contents lists available at SciVerse ScienceDirect

Applied Catalysis B: Environmental

journal homepage: www.elsevier.com/locate/apcatb

Preparation of calcium tantalum oxynitride from layered oxide precursors to improve photocatalytic activity for hydrogen evolution under visible light

Ryo Sasaki [a], Kazuhiko Maeda [a,b], Yoko Kako [a], Kazunari Domen [a,*]

[a] Department of Chemical System Engineering, The University of Tokyo, 7-3-1 Hongo, Bunkyo-ku, Tokyo 113-8656, Japan
[b] Precursory Research for Embryonic Science and Technology (PRESTO), Japan Science and Technology Agency (JST), 4-1-8 Honcho Kawaguchi, Saitama 332-0012, Japan

ARTICLE INFO

Article history:
Available online 20 October 2011

Keywords:
Layered oxide
Hydrogen production
Oxynitride
Photocatalyst
Visible light
Water splitting

ABSTRACT

A new precursor route to prepare calcium tantalum oxynitride ($CaTaO_2N$) was explored in an attempt to improve the photocatalytic activity for H_2 evolution from water under visible light. $CaTaO_2N$ catalysts were prepared using either a layered metal oxide (e.g., $RbCa_2Ta_3O_{10}$ or $HCa_2Ta_3O_{10}$) or a bulk-type Ca-Ta oxide prepared by the polymerized complex (PC) method. $CaTaO_2N$ samples prepared from the layered oxides had a less-aggregated morphology and a bluer absorption edge than an analog from a PC-derived precursor, in addition to a lower density of anionic defects. Samples prepared from the layered oxide also showed an enhanced photocatalytic activity for H_2 evolution from an aqueous methanol solution under visible light ($\lambda > 420$ nm), primarily because of their lower density of anionic defects and the enhanced driving force for surface redox reactions that resulted from their blue-shifted absorption edge.

1. Introduction

Photocatalytic water splitting using semiconductor particles and sunlight is a promising method of producing clean fuel from renewable resources, and many photocatalysts based on metal oxides have been investigated [1]. However, the large band gaps (>3 eV) of metal oxides restrict the utilization of visible light, which is the main component of the solar spectrum. Therefore, the development of stable photocatalysts that can respond to visible light is a central topic in the field of water splitting photocatalysis [1–4].

Our group previously reported that (oxy)nitrides are potential candidates for photocatalytic water splitting under visible light [3,4]. Compared to the conventional metal oxide photocatalysts, (oxy)nitrides have wide visible-light absorption bands at wavelengths ranging from 500 to 750 nm, depending on their principal cation component and the concentration of nitrogen. Some of these catalysts have achieved overall water splitting into H_2 and O_2 under visible light [5–10]. A common drawback of (oxy)nitrides for photocatalytic water-splitting applications, however, is their relatively low activity for water reduction. This low activity is attributable in part to the inherently high defect density of (oxy)nitrides and the lack of a suitable modification method to improve their reduction behavior [4,7,9]. It is therefore necessary to develop a new modification and/or preparation method that enhances the H_2 evolution activity of (oxy)nitrides. We have developed several approaches toward this objective, which include modification by a suitable nanoparticulate cocatalyst [6,11], post-treatment [10,12], surface modification by ZrO_2 nanoparticles [13,14], forming a solid solution with a wide-gap oxide [15], and reducing the particle size to the nanometer scale [16,17].

(Oxy)nitrides can be readily prepared by heating the corresponding metal oxide under a flow of NH_3 at high temperature. The resulting physicochemical properties, which greatly affect the photocatalytic activity, are dependent on the precursor employed. Using mesoporous C_3N_4 as a template, for example, it is possible to prepare nanoparticulate Ta_3N_5 with different particle sizes (7–22 nm) [17]. Nitridation of silica-coated mesoporous Ta_2O_5 with crystallized pore walls can yield mesoporous Ta_3N_5 [18]. The thus-obtained Ta_3N_5 photocatalysts exhibit an enhanced activity for H_2 evolution from water under visible light. For GaN–ZnO solid solutions, which are typically prepared from Ga_2O_3 and ZnO, the crystallinity of the ZnO precursor has a significant impact on the activity of the resulting GaN–ZnO for overall water splitting [19]. Thus, varying the oxide precursor for the synthesis of (oxy)nitrides can offer a simple means of improving the photocatalytic activity of a given (oxy)nitride.

In this paper, we report a new route for the preparation of the oxynitride $CaTaO_2N$ from layered metal oxide precursors ($RbCa_2Ta_3O_{10}$ and $HCa_2Ta_3O_{10}$). The resulting $CaTaO_2N$ catalyst demonstrated an enhanced activity for H_2 evolution under visible light. $CaTaO_2N$ was previously reported to exhibit water reduction activity under visible light, but the activity remains in need of improvement [20,21]. The structures of $RbCa_2Ta_3O_{10}$ and $CaTaO_2N$ are shown in Fig. 1. $RbCa_2Ta_3O_{10}$ is a layered perovskite compound that consists of three-layer perovskite slabs interleaved with

* Corresponding author. Tel.: +81 3 5841 1148; fax: +81 3 5841 8838.
E-mail address: domen@chemsys.t.u-tokyo.ac.jp (K. Domen).

0926-3373/$ – see front matter © 2011 Elsevier B.V. All rights reserved.
doi:10.1016/j.apcatb.2011.10.024

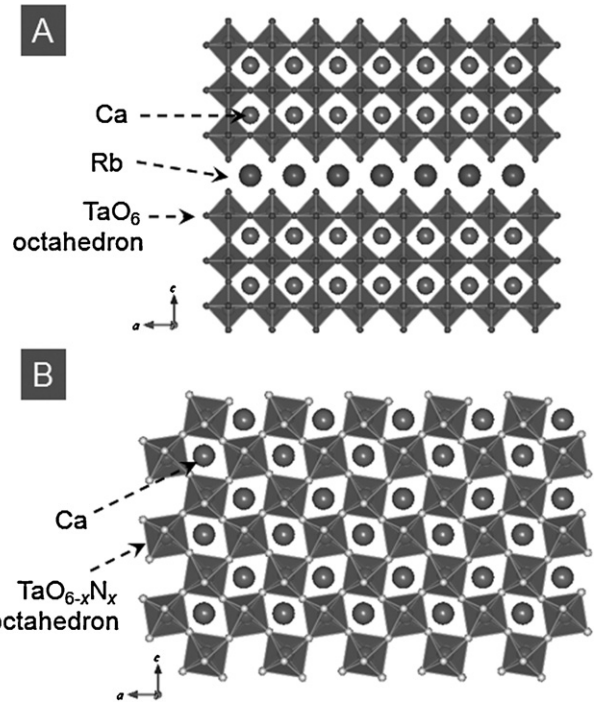

Fig. 1. Crystal structure of (A) $RbCa_2Ta_3O_{10}$, and (B) $CaTaO_2N$.

interlayer Rb^+ cations for charge compensation. $CaTaO_2N$, on the other hand, is a bulk-type compound with a perovskite-like structure.

2. Experimental

2.1. Preparation of photocatalysts

Layered $RbCa_2Ta_3O_{10}$ and $HCa_2Ta_3O_{10}$ were prepared as precursors for $CaTaO_2N$ by a conventional solid-state reaction method [22,23]. Stoichiometric amounts of $CaCO_3$ (Kanto Chemical, 99.5%) and Ta_2O_5 (High Purity Chemical, 99.9%) with 25% excess Rb_2CO_3 (Kanto Chemical, >97%) to compensate for the volatilization of Rb during preparation were mixed in a mortar. The mixture was precalcined at 1123 K for 12 h, and calcined at 1323 K for 12 h twice. $HCa_2Ta_3O_{10}$ was also prepared by shaking 2 g of the as-prepared $RbCa_2Ta_3O_{10}$ in aqueous nitric acid (1 M) at room temperature for 3 days with daily centrifugation and replacement of the acid solution. The product was isolated by centrifugation, washing, and finally drying at 343 K in an oven overnight.

For nitridation to obtain $CaTaO_2N$, $CaCO_3$ was mixed with the as-prepared $RbCa_2Ta_3O_{10}$ or $HCa_2Ta_3O_{10}$ to compensate for the lack of Ca, and the mixture was then subjected to nitridation under an NH_3 flow (100 mL min^{-1}) at 1173 K for 20 h. The nitrided products derived from $RbCa_2Ta_3O_{10}$ and $HCa_2Ta_3O_{10}$ are represented hereafter as L(Rb)-$CaTaO_2N$ and L(H)-$CaTaO_2N$, respectively. $CaTaO_2N$ was also synthesized by nitriding a bulk-type Ca-Ta oxide that was previously prepared by the PC method [24]. The PC-derived Ca-Ta oxide was nitrided under the same conditions, and the resulting material is referred to as B-$CaTaO_2N$ hereafter.

Pt was loaded as a cocatalyst for water reduction onto the $CaTaO_2N$ by an impregnation method from aqueous H_2PtCl_6 solution followed by heat-treatment at 473 K under an H_2 flow for 1 h.

2.2. Characterization of catalysts

The prepared samples were characterized by powder X-ray diffraction (XRD; RINT-UltimaIII + D/Tex Ultra UltimaIII detector, Rigaku; Cu Kα), scanning electron microscopy (SEM; S-4700, Hitachi), energy-diffuse X-ray analysis (EDX, Emax-7000, Horiba), and ultraviolet–visible diffuse reflectance spectroscopy (UV–vis. DRS; V-670, Jasco). The Brunauer, Emmett, Teller (BET) surface area was measured using a BELSORP-mini instrument (BEL Japan) at liquid nitrogen temperature. The amount of anions contained in the sample was determined using an oxygen/nitrogen/hydrogen combustion analyzer (EMGA-620W/C; Horiba).

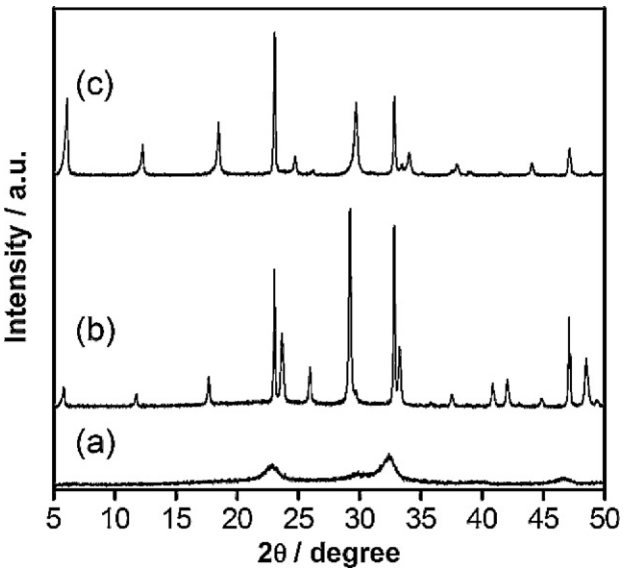

Fig. 2. XRD patterns of (a) bulk-type Ca-Ta oxide prepared by the PC method, (b) $RbCa_2Ta_3O_{10}$, and (c) $HCa_2Ta_3O_{10}$.

2.3. Photocatalytic reactions

Photocatalytic reactions were carried out in a Pyrex top-irradiation reaction vessel connected to a glass closed gas circulation system. The photoreduction of protons to H_2 was performed using an aqueous methanol solution (20 vol%, 100 mL) containing 0.1 g of the catalyst. The solution was evacuated before the reaction to ensure that no air remained in the vessel. The solution was irradiated using a Xe lamp (300 W) fitted with a cutoff filter and a water filter to eliminate light in the UV and infrared regions, respectively, and to select only light at visible wavelengths ($\lambda > 420$ nm). The reactant solution was maintained at room temperature by flowing water during the reaction. The evolved gases were analyzed by gas chromatography.

3. Results and discussion

3.1. Structural properties of the precursors

As shown in Fig. 2, XRD analysis indicated that the bulk Ca-Ta oxide prepared by the PC method exhibited a broad profile, indicative of a less-crystallized oxide sample. On the other hand, the diffraction patterns of the as-prepared $RbCa_2Ta_3O_{10}$ and $HCa_2Ta_3O_{10}$ were consistent with the reported data [22,23], indicating the successful preparation of the layered solids. Fig. 3 shows SEM images of the bulk Ca-Ta oxide and the layered oxides. The bulk Ca-Ta oxide consisted of aggregated particles that in turn consisted of fine primary particles (Fig. 3(a)). $RbCa_2Ta_3O_{10}$ and $HCa_2Ta_3O_{10}$, on the other hand, consisted of plate-like particles ranging from 0.5 to 3 μm in size, reflecting the original layered structure. Both of these oxide powders were white, indicating no visible-light absorption capability. The band gaps of these metal oxides have been reported to be larger than 4 eV [1].

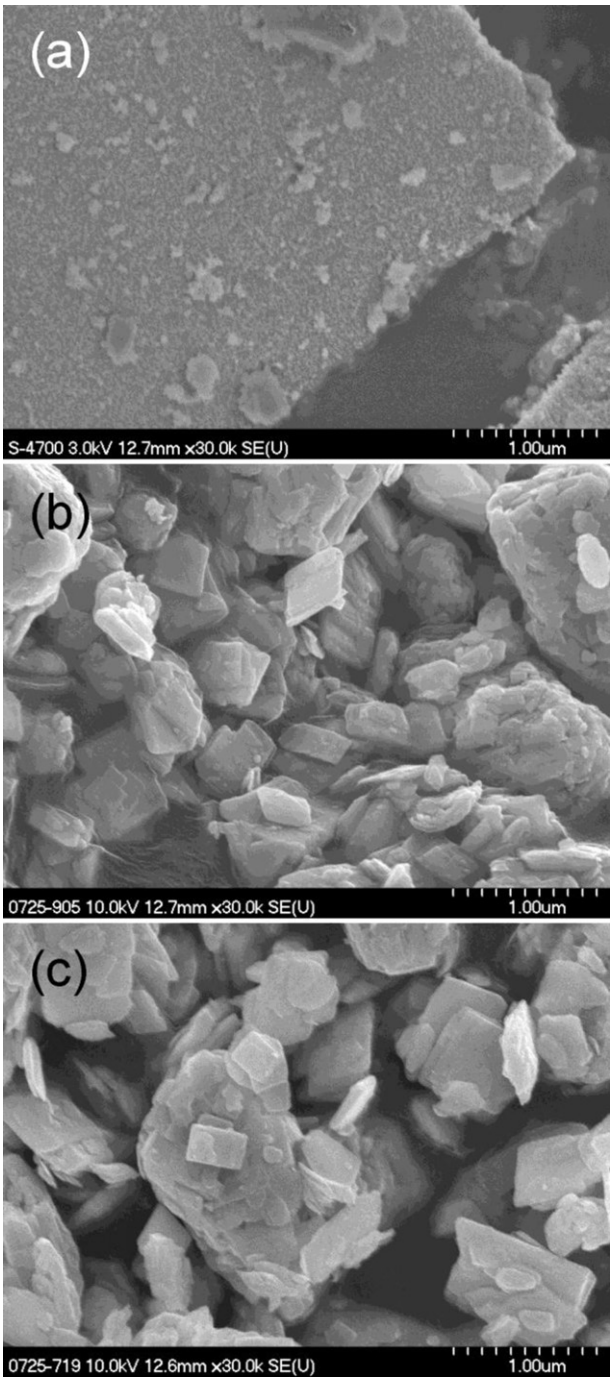

Fig. 3. SEM images of (a) bulk-type Ca-Ta oxide prepared by the PC method, (b) $RbCa_2Ta_3O_{10}$, and (c) $HCa_2Ta_3O_{10}$.

3.2. Characterization of nitrided samples

Fig. 4 shows XRD patterns of the corresponding nitrided products. All samples exhibited single-phase diffraction patterns similar to a perovskite-like structure, with no impurity phases. The diffraction peaks exhibited by L(Rb)-$CaTaO_2N$ and L(H)-$CaTaO_2N$ (lines (b) and (c)) were slightly broader than those of B-$CaTaO_2N$ (line (a)), indicating smaller crystallite sizes in the L(Rb)-$CaTaO_2N$ and L(H)-$CaTaO_2N$ samples. SEM images of the nitrided samples are shown in Fig. 5. As reported previously, B-$CaTaO_2N$ retained a highly aggregated form with constituent particles 50–100 nm in diameter [21]. L(Rb)-$CaTaO_2N$ and L(H)-$CaTaO_2N$ particles also aggregated to form larger secondary particles (>1 μm). However, the degree of

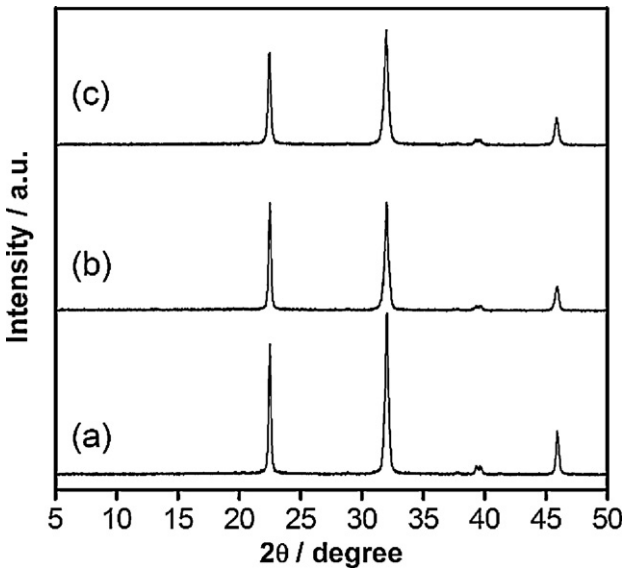

Fig. 4. XRD patterns of (a) B-$CaTaO_2N$, (b) L(Rb)-$CaTaO_2N$, and (c) L(H)-$CaTaO_2N$.

Table 1
Absorption edge and oxygen and nitrogen content of $CaTaO_2N$ samples.

Sample	Absorption edge (nm)	Anion content (wt%)			
		O	N	O/N	O+N
Ideal $CaTaO_2N$	–	12.0	5.2	2.3	17.2
B-$CaTaO_2N$	505	9.8	5.7	1.7	15.5
L(Rb)-$CaTaO_2N$	485	11.6	4.6	2.5	16.2
L(H)-$CaTaO_2N$	495	11.2	5.1	2.2	16.3

aggregation was less pronounced than that of B-$CaTaO_2N$ (Fig. 5(b) and (c)). The specific surface areas of the B-$CaTaO_2N$, L(Rb)-$CaTaO_2N$, and L(H)-$CaTaO_2N$ samples were 9.6, 8.9, and 8.7 $m^2\ g^{-1}$, respectively. Furthermore, no Rb ions were detected in the L(Rb)-$CaTaO_2N$ samples by EDX. Presumably, any Rb ions existing in the interlayer space of $RbCa_2Ta_3O_{10}$ underwent volatilization during nitridation.

Ultraviolet–visible diffuse reflectance spectra for the same samples are shown in Fig. 6. The absorption band edge of B-$CaTaO_2N$ (spectrum (a)) appeared at ca. 500 nm, and was most likely due to an electron transition from the valence band formed by N 2p orbitals to the conduction band consisting of empty Ta 5d orbitals. The increase in the background level (longer than 500 nm) of the B-$CaTaO_2N$ spectrum is attributable to the presence of reduced tantalum species [13–17], suggesting the presence of defects that acted as recombination centers for photogenerated carriers. The absorption edges of L(Rb)-$CaTaO_2N$ and L(H)-$CaTaO_2N$ (spectra (b) and (c)) were blue-shifted, compared to B-$CaTaO_2N$, and their background level was less pronounced. The blue-shift and the reduction of the background level were more pronounced in L(Rb)-$CaTaO_2N$ than in L(H)-$CaTaO_2N$.

To investigate the reason for the different absorption profiles of these $CaTaO_2N$ samples, their oxygen and nitrogen contents were measured. Table 1 lists the anion content of the $CaTaO_2N$ samples, as well as the absorption edges that were estimated from the onset wavelength of UV–vis. DRS. In B-$CaTaO_2N$, the amounts of oxygen and nitrogen were smaller and larger, respectively, than those expected from the stoichiometry of $CaTaO_2N$. Furthermore, the total anion content (O + N) was less than the ideal value (17.2). This indicates that the B-$CaTaO_2N$ was non-stoichiometric, and suggests that the B-$CaTaO_2N$ contained a considerable number of defect sites. L(Rb)-$CaTaO_2N$ and L(H)-$CaTaO_2N$ contained more anions than B-$CaTaO_2N$, although the oxygen and nitrogen amounts

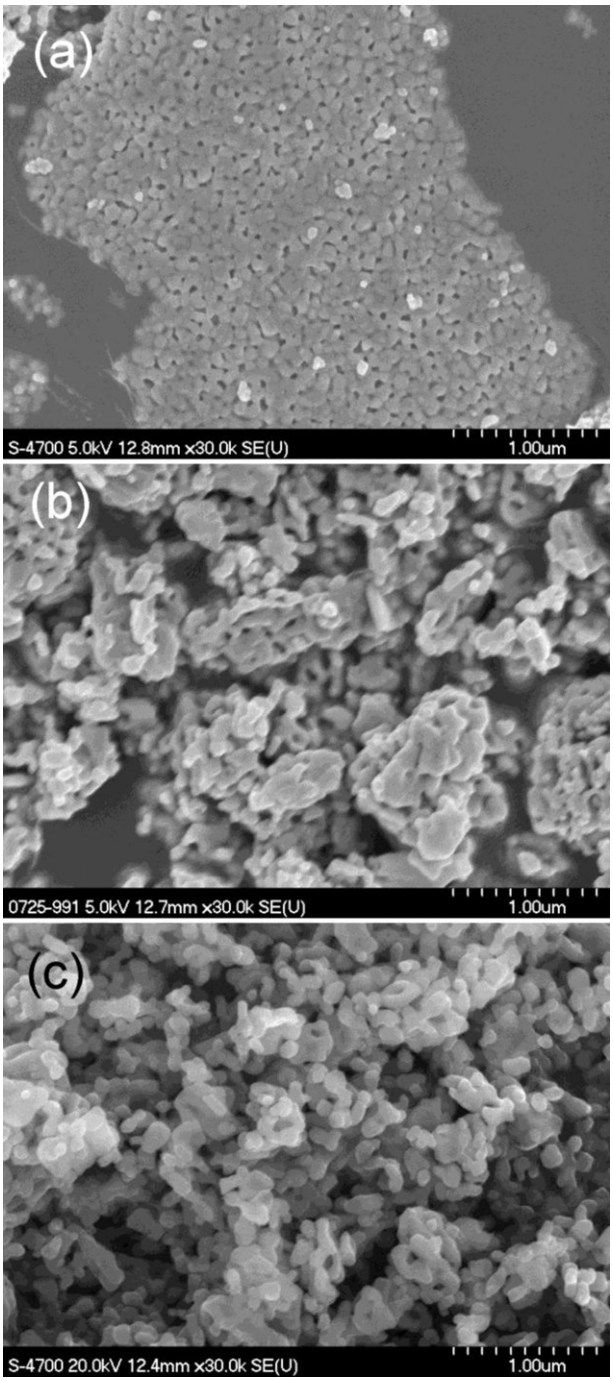

Fig. 5. SEM images of (a) B-$CaTaO_2N$, (b) L(Rb)-$CaTaO_2N$, and (c) L(H)-$CaTaO_2N$.

were larger and smaller, respectively. It has been reported that the tops of the valence bands of tantalum (oxy)nitrides are shifted to higher potential energies with increasing nitrogen concentration, due to the increased population of N2p orbitals that comprise the valence band tops [3]. Similarly, the position of the absorption edge of non-stoichiometric $CaTaO_2N$ would be affected by the nitrogen concentration. It thus appears in this case that the lower nitrogen concentration in L(Rb)-$CaTaO_2N$ and L(H)-$CaTaO_2N$ contributes to the apparent blue-shift in the absorption edge position, as compared to B-$CaTaO_2N$. The degree of the blue-shift in the absorption edge was consistent with the amount of nitrogen in the $CaTaO_2N$ samples; that is, the lower the nitrogen content, the larger the blue-shift. The weaker background level in

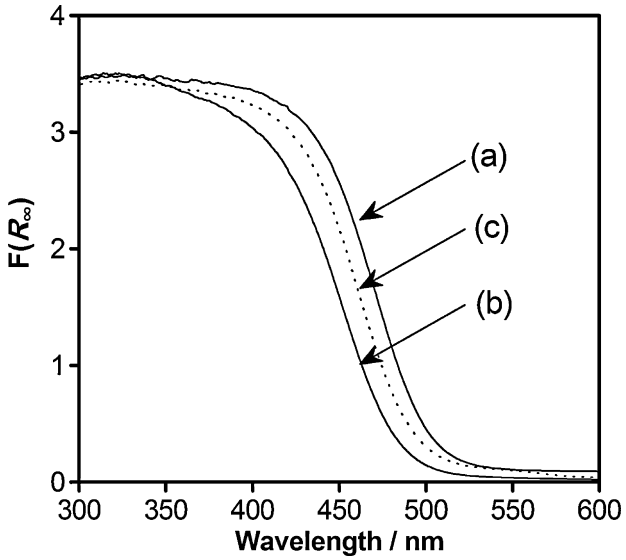

Fig. 6. UV–visible DRS of (a) B-$CaTaO_2N$, (b) L(Rb)-$CaTaO_2N$, and (c) L(H)-$CaTaO_2N$.

L(Rb)-$CaTaO_2N$ and L(H)-$CaTaO_2N$ can also be explained by the elemental analysis results, which revealed that these samples contained less anionic vacancies than the B-$CaTaO_2N$ did (Table 1).

3.3. Photocatalytic activity

The rates of H_2 evolution from aqueous methanol solution using 0.3 wt% Pt-loaded samples under visible light ($\lambda > 420$ nm) are listed in Table 2. All of the catalysts exhibited visible-light photocatalytic activity, and no reaction took place in the dark. However, the rates of H_2 evolution from L(Rb)-$CaTaO_2N$ and L(H)-$CaTaO_2N$ were 2–2.8 times that of B-$CaTaO_2N$, and L(Rb)-$CaTaO_2N$ exhibited the highest activity. N_2 evolution, which has sometimes been observed for other (oxy)nitride photocatalysts during water splitting reactions, and indicates the oxidative decomposition of (oxy)nitrides [3], was undetectable in all cases. Even at the optimal Pt-loading conditions, L(Rb)-$CaTaO_2N$ exhibited a higher activity (0.3 wt% Pt, 8.3 $\mu mol\ h^{-1}$) than B-$CaTaO_2N$ did (0.1 wt% Pt, 4.8 $\mu mol\ h^{-1}$). Thus, $CaTaO_2N$ prepared from layered Ca-Ta oxides was found to be superior to that obtained from a bulk-type Ca-Ta oxide.

Particle morphology, absorption band position (i.e., band gap energy), and defect density are all considered to be possible factors affecting the H_2 evolution activity of $CaTaO_2N$ photocatalysts. Table 2 lists some of the physicochemical properties and the H_2 evolution activities of the prepared $CaTaO_2N$ samples. Although the wider absorption band of B-$CaTaO_2N$ appears to be advantageous, the photocatalytic activity of this material was lower than that of L(Rb)-$CaTaO_2N$ and L(H)-$CaTaO_2N$. The more pronounced background level at longer wavelengths (spectrum (a), Fig. 6) and the elemental analysis results (Table 1) suggest that B-$CaTaO_2N$ had a higher defect density than L(Rb)-$CaTaO_2N$ and L(H)-$CaTaO_2N$, and the resulting reduction in activity was likely to conceal the (possible) positive effects derived from the wider visible light absorption band of the nanoparticulate material.

The use of layered $RbCa_2Ta_3O_{10}$ or $HCa_2Ta_3O_{10}$ as a precursor, on the other hand, resulted in an improvement of activity. The density of defects was lower in the as-obtained L(Rb)-$CaTaO_2N$ and L(H)-$CaTaO_2N$, as indicated by the weakened background level at longer wavelengths (Fig. 6) and the elemental analysis results (Table 1). It is likely that reducing the density of defects contributed to the higher activity of L(Rb)-$CaTaO_2N$ and L(H)-$CaTaO_2N$, even though the absorption band edges of the materials were located at a wavelength 10–20 nm shorter than that of B-$CaTaO_2N$. According

Table 2
Photocatalytic activities[a] and physicochemical properties of $CaTaO_2N$ samples.

Sample	Activity[b] (μmol h^{-1})	Specific surface area (m^2 g^{-1})	Absorption edge (nm)	Relative background absorption[c]
B-$CaTaO_2N$	3.0	9.6	505	Stronger
L(Rb)-$CaTaO_2N$	8.3	8.9	485	Weaker
L(H)-$CaTaO_2N$	5.9	8.7	495	Weaker

[a] Reaction conditions: catalyst, 0.1 g (0.3 wt% Pt loaded); light source, xenon lamp (300 W) with cutoff filter; reaction vessel, top-irradiation type.
[b] Initial rate of H_2 evolution from aqueous methanol solution (20 vol%, 100 mL).
[c] Judged from the absorption background level at wavelengths longer than 500 nm (Fig. 6).

to our recent kinetic study on water splitting over a GaN–ZnO photocatalyst [25], for n-type semiconductors such as $CaTaO_2N$ in which the presence of anionic defects is the origin of the n-type semiconducting character, reducing n-type semiconducting property (in other words, reducing the density of anionic defects) lowers the possibility of recombination between intrinsic electrons and surface holes. As a result, an enhanced photocatalytic activity can be obtained. This has been evidenced by ZrO_2-modified TaON photocatalyst, which has an enhanced activity for water reduction [13,14]. In addition to the reduced density of defects, the blue-shifted absorption edge of L(Rb)-$CaTaO_2N$ and L(H)-$CaTaO_2N$ might have a positive effect on photocatalytic activity because it leads to an enhanced driving force for surface redox reactions. This idea is supported by the observation that the order of activity enhancement in $CaTaO_2N$ samples was consistent with that of the blue-shift of the absorption edge.

Another factor that can affect photocatalytic activity is the morphology of $CaTaO_2N$. The effect of particle morphology on activity has been reported for $SnNb_2O_6$, which also catalyzes H_2 evolution from aqueous methanol solution under visible light [26]. In that study, it was claimed that smoother and more isolated particles are advantageous for efficient H_2 evolution. Therefore, the less-aggregated morphologies of the present L(Rb)-$CaTaO_2N$ and L(H)-$CaTaO_2N$ materials may have an additional positive impact on their activity.

4. Conclusion

$CaTaO_2N$ was successfully prepared by nitriding a mixture of layered Ca-Ta oxide ($RbCa_2Ta_3O_{10}$ or $HCa_2Ta_3O_{10}$) and $CaCO_3$ under NH_3 flow. The as-prepared $CaTaO_2N$ consisted of aggregated nanoparticles with a primary particle size of 50–100 nm, and had a lower density of anionic defects. Compared to $CaTaO_2N$ prepared from a bulk-type Ca-Ta oxide, $CaTaO_2N$ derived from the layered oxides exhibited an enhanced photocatalytic activity for H_2 evolution under visible light. Since the preparation of $CaTaO_2N$ from layered oxides resulted in an improvement in its photocatalytic activity, the improvement of other oxynitrides by the same method is currently under investigation.

Acknowledgements

This work was supported by the Research and Development in a New Interdisciplinary Field Based on Nanotechnology and Materials Science program of the Ministry of Education, Culture, Sports, Science and Technology (MEXT) of Japan, and The KAITEKI Institute, Inc. Acknowledgement is extended to a Grant-in-Aid for Young Scientists (Start-up) (No. 21850009) from the Japan Society for the Promotion of Science (JSPS) and a PRESTO/JST program.

References

[1] A. Kudo, Y. Miseki, Chem. Soc. Rev. 38 (2009) 253–278.
[2] J.S. Lee, Catal. Surv. Asia 9 (2005) 217–227.
[3] K. Maeda, K. Domen, J. Phys. Chem. C 111 (2007) 7851–7861.
[4] K. Maeda, K. Domen, J. Phys. Chem. Lett. 1 (2010) 2655–2661.
[5] K. Maeda, T. Takata, M. Hara, N. Saito, Y. Inoue, H. Kobayashi, K. Domen, J. Am. Chem. Soc. 127 (2005) 8286–8287.
[6] K. Maeda, K. Teramura, D. Lu, T. Takata, N. Saito, Y. Inoue, K. Domen, Nature 440 (2006) 295.
[7] K. Maeda, H. Hashiguchi, H. Masuda, R. Abe, K. Domen, J. Phys. Chem. C 112 (2008) 3447–3452.
[8] Y. Lee, H. Terashima, Y. Shimodaira, K. Teramura, M. Hara, H. Kobayashi, K. Domen, M. Yashima, J. Phys. Chem. C 111 (2007) 1042–1048.
[9] F. Tessier, P. Maillard, Y. Lee, C. Bleugat, K. Domen, J. Phys. Chem. C 113 (2009) 8526–8531.
[10] K. Takanabe, T. Uzawa, X. Wang, K. Maeda, M. Katayama, J. Kubota, A. Kudo, K. Domen, Dalton Trans. (2009) 10055–10062.
[11] M. Hara, J. Nunoshige, T. Takata, J.N. Kondo, K. Domen, Chem. Commun. 300 (2003) 0–3001.
[12] Y. Lee, K. Nukumizu, T. Watanabe, T. Takata, M. Hara, M. Yoshimura, K. Domen, Chem. Lett. 35 (2006) 352–353.
[13] K. Maeda, H. Terashima, K. Kase, M. Higashi, M. Tabata, K. Domen, Bull. Chem. Soc. Jpn. 81 (2008) 927–937.
[14] K. Maeda, M. Higashi, D. Lu, R. Abe, K. Domen, J. Am. Chem. Soc. 132 (2010) 5858–5868.
[15] K. Maeda, H. Terashima, K. Kase, K. Domen, Appl. Catal. A: Gen. 357 (2009) 206–212.
[16] K. Maeda, N. Nishimura, K. Domen, Appl. Catal. A: Gen. 360 (2009) 88–92.
[17] L. Yuliati, J.-H. Yang, X. Wang, K. Maeda, T. Takata, M. Antonietti, K. Domen, J. Mater. Chem. 20 (2010) 4295–4298.
[18] T. Hisatomi, M. Otani, K. Nakajima, K. Teramura, Y. Kako, D. Lu, T. Takata, J.N. Kondo, K. Domen, Chem. Mater. 22 (2010) 3854–3861.
[19] K. Maeda, K. Domen, Chem. Mater. 22 (2010) 612–623.
[20] D. Yamasita, T. Takata, M. Hara, J.N. Kondo, K. Domen, Solid State Ionics 172 (2004) 591–595.
[21] M. Higashi, R. Abe, T. Takata, K. Domen, Chem. Mater. 21 (2009) 1543–1549.
[22] K. Toda, M. Sato, J. Mater. Chem. 6 (1996) 1067–1071.
[23] M. Machida, T. Mitsuyama, K. Ikeue, S. Matsushima, M. Arai, J. Phys. Chem. B 109 (2005) 7801–7806.
[24] M. Kakihana, M. Milanova, M. Arima, T. Okubo, M. Yashima, M. Yoshimura, J. Am. Ceram. Soc. 79 (1996) 1673–1676.
[25] T. Hisatomi, K. Maeda, K. Takanabe, J. Kubota, K. Domen, J. Phys. Chem. C 113 (2009) 21458–21466.
[26] Y. Hosogi, Y. Shimodaira, H. Kato, H. Kobayashi, A. Kudo, Chem. Mater. 20 (2008) 1299–1307.